

Supporting Information for:

A facile synthetic route for highly durable mesoporous platinum thin film electrocatalysts based on graphene: morphological and support effects on the oxygen reduction reaction

Kie Yong Cho,^{a,b} Yong Sik Yeom,^a Heun Young Seo,^a Pradip Kumar,^c Kyung-Youl Baek^{b,d} and Ho Gyu Yoon^{a,e,*}

^a Department of Materials Science and Engineering, Korea University, Seoul 02841, Korea.

^b Materials Architecturing Research Center, Korea Institute of Science and Technology, Seoul 02792, Korea.

^c Chemistry Division, Bhabha Atomic Research Centre, Mumbai 400085, India.

^d Nanomaterials Science and Engineering, University of Science and Technology, Daejeon 34113, Korea.

^e Graduate School of Management of Technology, Korea University, Seoul 02841, Korea.

*Corresponding Author: hgyoon@korea.ac.kr (H. G. Yoon)

List of Supporting Information

Experimental Section – 2 p

Calculation of the Average Crystalline Size – 5 p

Calculation of Specific ECSA, Electron-transfer Number, and ORR Activities – 5 p

Supporting Figures – 8 p

References – 23 p

Experimental Section

Preparation of IPG support: IPG was fabricated according to our previous reports, as follows:¹ pyrene-functionalized poly(dimethylaminoethyl methacrylate)-*b*-poly[(ethylene glycol) methyl ether methacrylate] (Py-PDMAEMA-*b*-PPEGMEMA) ionic polymer (Mn:19k, PDI: 1.09, 16 wt% of PDMAEMA) was synthesized by a combination of atom transfer radical polymerization (ATRP) and quaternization reaction methods (Scheme S1). rGO was synthesized by reacting GO with hydrazine monohydrate at 80°C for 12 h after synthesizing GO by a modified Hummer's method. The obtained rGO (30 mg) was dispersed in 200 mL of N-methyl-2-pyrrolidone (NMP) by sonication for 30 min. Subsequently, the ionic block copolymer (80 mg) was added to the rGO suspension, which was then stirred overnight. Next, the mixture was sonicated for 20 min. Well-dispersed IPG were obtained, and the free ionic block copolymer was removed by simple filtration under reduced pressure and washing with acetone. The obtained powdery products were dried at RT for an hour under reduced pressure. The resulting product exhibited that the introduced ionic polymer was proximity 50 wt% in IPG, derived from TGA analysis.

Synthesis of MPt/IPG and Pt/IPG Catalysts: The IPG support (0.4 mg, IPG) was dispersed in 13 mL of N,N-dimethylformamide (DMF, Sigma-Aldrich, >99%) by sonication for 5 min. BA (10 mg, Sigma-Aldrich, >99.5%) and PVP (85 mg, Sigma-Aldrich, 10k g/mol) were sequentially added to the IPG solution, which was then subjected to sonication for 10 min. Subsequently, this solution was placed in an ice bath and agitated for 10 min. After the foregoing procedure, H₂PtCl₆ aqueous solution (2mL, 20 mM in water, Sigma-Aldrich, 99.995%) was injected to the prepared solution, and vigorously agitated in the ice bath for 10 sec. The reaction was allowed to continue at 130 °C for 30 min. Thereafter, the reaction solution was placed in an ice bath and stirred for 10 min. The crude solution was purified by centrifugation 3 times using a mixture of ethanol and acetone (2:1). The obtained precipitates were dispersed in 100 mL of tetrahydrofuran (THF) by sonication for 10 min, and the

products were collected by filtration under reduced pressure. The filtered powder was dispersed in acetic acid and treated at 60 °C for 1h to remove the organic contamination. The resulting products was acquired by filtration and then dried at room temperature under reduced pressure for 24 h. The Pt/IPG was prepared by the similar synthetic protocols used for the MPt/IPG except for only changing the morphology forming agent, the only use and PVP (85 mg, Sigma-Aldrich, 10k g/mol). The moropholgical and compositional evaluations were displayed in Fig. S5B (53.2 wt% of Pt).

Synthesis of Pt/rGO Catalyst: Reduced graphene oxide (0.4 mg, IPG) was dispersed in 13 mL of DMF by sonication for 60 min. BA (10 mg, Sigma-Aldrich, >99.5%) and PVP (85 mg, Sigma-Aldrich, 10k g/mol) was sequentially added to IPG solution, followed by sonication for 10 min. Thereafter, this solution was placed on an ice bath and agitated for 10 min. After the foregoing procedure, H₂PtCl₆ aqueous solution (2mL, 20 mM in water, Sigma-Aldrich, 99.995%) was injected to the prepared solution, and strongly agitated in the ice bath for 10 sec. The reaction was retained at 130 °C for 30 min. Then, the reaction solution was placed in an ice bath and stirred for 10 min. The crude solution was purified by centrifugation 3 times using a mixture of ethanol and acetone (2:1). The obtained precipitates were dispersed in 100 mL of THF by sonication for 10 min and resulting products were obtained by filtration under reduced pressure. The filtered powder was dried at room temperature under reduced pressure for 24 h.

AFM Sample Preparation: AFM samples were prepared using a spin-coating method. Silicon wafer was washed with acetone at 100 °C for 30 min and then dried at RT under vacuum for 30 min. Thereafter, the UVO treatment was followed for 30 min. Upon completing UVO treatment, the silicon wafer was applied for spin-coating (1000 rpm, 10 sec) using the catalyst solution in methanol (0.01 mg/mL). The acquired AFM sample was dried at 50 °C under vacuum for an hour.

Electrochemical Characterization: ORR measurements were performed using a three-electrode system composed of a glassy carbon rotating disk electrode (RDE) (diameter: 3 mm, area: 0.0706 cm²) as a working electrode, Ag/AgCl (3 M KCl) as a reference electrode, and Pt mesh (1 × 1 cm²) as a counter electrode. The reference electrode was converted to a reversible hydrogen electrode (RHE). The RHE calibration was conducted in a H₂-saturated electrolyte with platinum wire as a working electrode. The potential was swept near the thermodynamic potential (-0.268V) for the H⁺/H₂ reaction and calculated using E(RHE)=E(Ag/AgCl)+0.268V.² The optimal quantity of catalyst was dispersed in a solution including 2-propanol (412.16 μL), water (82.43 μL), and 5 wt% Nafion solution (5.41 μL). The prepared catalyst solution was drop-casted on a glassy carbon electrode, and then the Pt contents in loaded catalysts were as follows: Pt/C: ~13.9 μg cm⁻², Pt/rGO: ~6.7 μg cm⁻², and MPt/IPG: ~3.7 μg cm⁻². The Pt loading masses of all catalysts were determined after optimizing the ORR conditions. CV curves were collected between 0.03 and 1.2 V_{RHE} using a scan rate 50 mV s⁻¹ in Ar-saturated 0.1 M HClO₄, and ORR polarization curves were measured at a scan rate 10 mV s⁻¹ and a rotation rate of 1600 rpm in O₂-saturated 0.1 M HClO₄ with electrolyte resistance correction. The ADTs were performed in the potential range of 0.6 and 1.1 V_{RHE} at 50 mV s⁻¹ for up to 30,000 cycles in O₂-saturated 0.1 M HClO₄.

Characterizations: The catalysts were characterized using Raman spectrometry (LabRam ARAMIS IR2, Horiba, Japan), XPS (X-TOOL, ULVAC-PHI) with a monochromatic AlK α source, STEM (FEI Talos F200X and FEI Titan 80-300™) equipped with EDX, tapping mode AFM (Multimode 8 with Nanoscope V controller, Veeco) equipped with an E-type vertical engage scanner, inductively coupled plasma atomic emission spectroscopy (ICP-AES, Varian, 710 ES), and XRD (Rigaku Smart Lab, Rigaku Co., Japan) using monochromatic CuK α X-rays. Electrochemical measurements were performed using a

glassy carbon RDE (ALS. Co., Ltd, RRDE-3A, Japan) connected to a potentiostat (VSP-300, Bio Logic Science Instruments, France).

Calculation of the Average Crystalline Size

The average crystalline size of Pt NPs in MPt/IPG was calculated by the Scherrer formula-derived Equation:

$$D_{av} = \frac{K\lambda}{\beta_{hkl}\cos\theta} \quad (S1)$$

where D_{av} is the average crystalline size, K is shape factor (0.9), λ is wavelength of $\text{CuK}\alpha$ radiation, and β_{hkl} is full width of half maximum (FWHM).

Table S1. Structural parameters of MPt/IPG

Catalyst	2θ	d (nm)	hkl	FWHM (rad)	D_{av}^a (nm)	D_{TEM}^b (nm)
MPt/IPG	39.7	0.22	(111)	0.04704	5.4	~5.0

^a D_{av} was deduced from Scherrer formula. ^b D_{TEM} was measured using STEM images.

Calculation of Specific ECSA, Electron-transfer Number, and ORR Activities

Calculation of specific ECSA: To derive the specific ECSA value, CV measurements were performed by cycling between 0.03 and 1.2 V_{RHE} at a scan rate of 50 mV s^{-1} in the 0.1 M HClO_4 aqueous solution after purging with Ar. The collected CV curves were used to determine the hydrogen desorption charge (Q_H) derived according to Equation S2:³

$$Q_H[C] = \int_{0.00}^{0.37} \frac{I[A] \times dE[V]}{v[V/s]} \quad (S2)$$

where C is the charge, I is the current, E is the potential, v is the scan rate, and Q is the charge in the hydrogen desorption area obtained after double-layer correction. The specific ECSA value was then calculated via Equation S3:⁴

$$\text{Specific ECSA} = \frac{Q_H}{m \times q_H} \quad (\text{S3})$$

where Q_H is the charge for hydrogen desorption, m is the loading amount of catalyst (metal and support), and q_H is the charge required for the monolayer adsorption of hydrogen on a Pt surface (210 $\mu\text{C}/\text{cm}^2$).

Calculation of electron-transfer number (n): To derive the electron-transfer number, the ORR polarization curves were measured in O_2 -saturated 0.1 M HClO_4 aqueous solution at a potential scan rate (10 mV s^{-1}) and at different rotation rates (200, 400, 800, 1600, and 2400 rpm). The K-L plots (J^{-1} vs. $\omega^{-1/2}$) of all catalysts at different potentials were applied to determine their fitted slope values (k). The electron-transfer number (n) was calculated according to Equation S4:^{3,4}

$$n = \frac{1}{0.62kFD_{\text{O}_2}^{2/3}\eta^{-1/6}C_{\text{O}_2}} \quad (\text{S4})$$

where k is the fitted slope from the K-L plots, F is the Faraday constant ($F = 96485.34 \text{ C mol}^{-1}$), D_0 is the diffusion coefficient of O_2 in 0.1 M HClO_4 ($1.93 \times 10^{-5} \text{ cm}^2 \text{ s}^{-1}$), η is the kinematic viscosity of the electrolyte ($1.009 \times 10^{-2} \text{ cm}^2 \text{ s}^{-1}$), and C_0 is saturation concentration of O_2 in 0.1 M HClO_4 at 1atm O_2 pressure ($1.16 \times 10^{-6} \text{ mol cm}^{-3}$). These parameters are determined at 293 K.

Calculation of specific and mass activity ($j_{k,\text{specific}}$ and $j_{k,\text{mass}}$, respectively): To derive the specific and mass activities, the ORR polarization curves were measured in the O_2 -

saturated 0.1 M HClO₄ aqueous solution at a potential scan rate of 10 mV s⁻¹ and a rotation rate of 1600 rpm, and then the kinetic current (*i_k*) was calculated from the K-L equation (Equation S5) as follows:

$$\frac{1}{i} = \frac{1}{i_k} + \frac{1}{i_d} \quad (\text{S5})$$

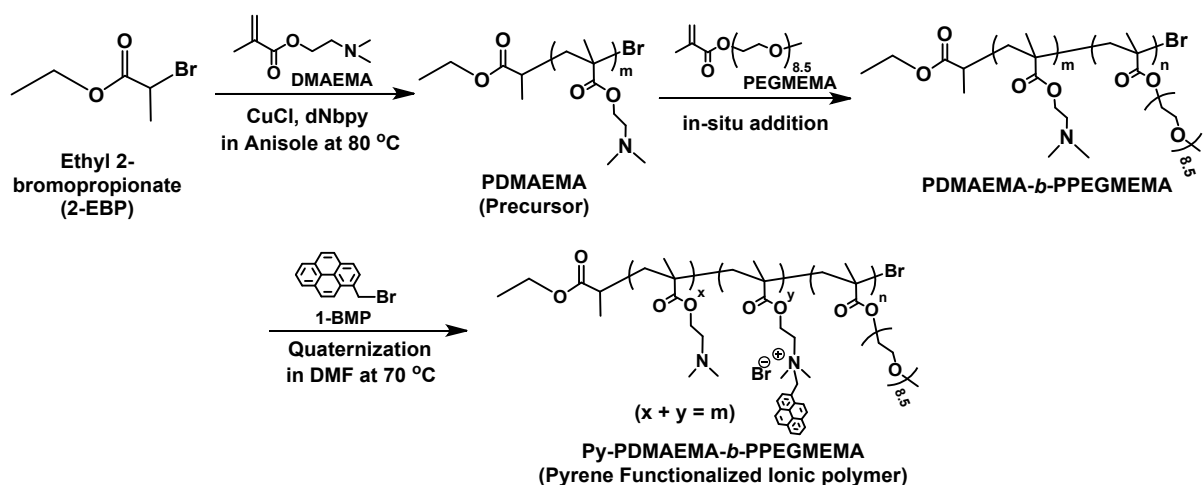
where *i* is the measured current and *i_d* is the diffusion limiting current. Based on ECSA, the specific activity was calculated according to Equation S6.³

$$j_{k,specific} = i_k \times \frac{q_H}{Q_H} \quad (\text{S6})$$

Based on the catalyst loading mass, the mass activity was calculated using Equation S7.

$$j_{k,mass} = \frac{i_k}{m} \quad (\text{S7})$$

where *m* is the Pt or catalyst (Pt and support) loading mass.



Scheme S1. Synthesis of pyrene functionalized PDMAEMA-*b*-PPEGMEMA ionic polymer.

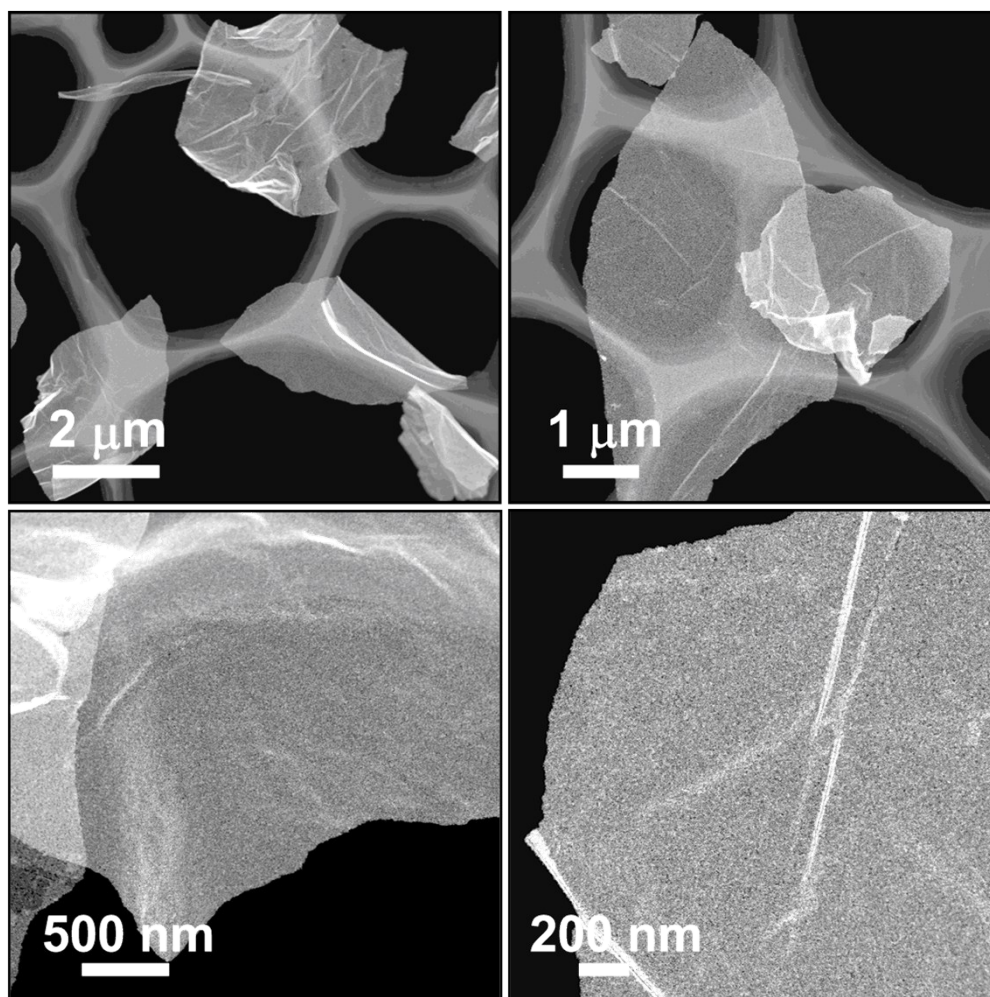


Fig. S1 Representative HAADF-STEM images of MPT/IPG at different magnifications.

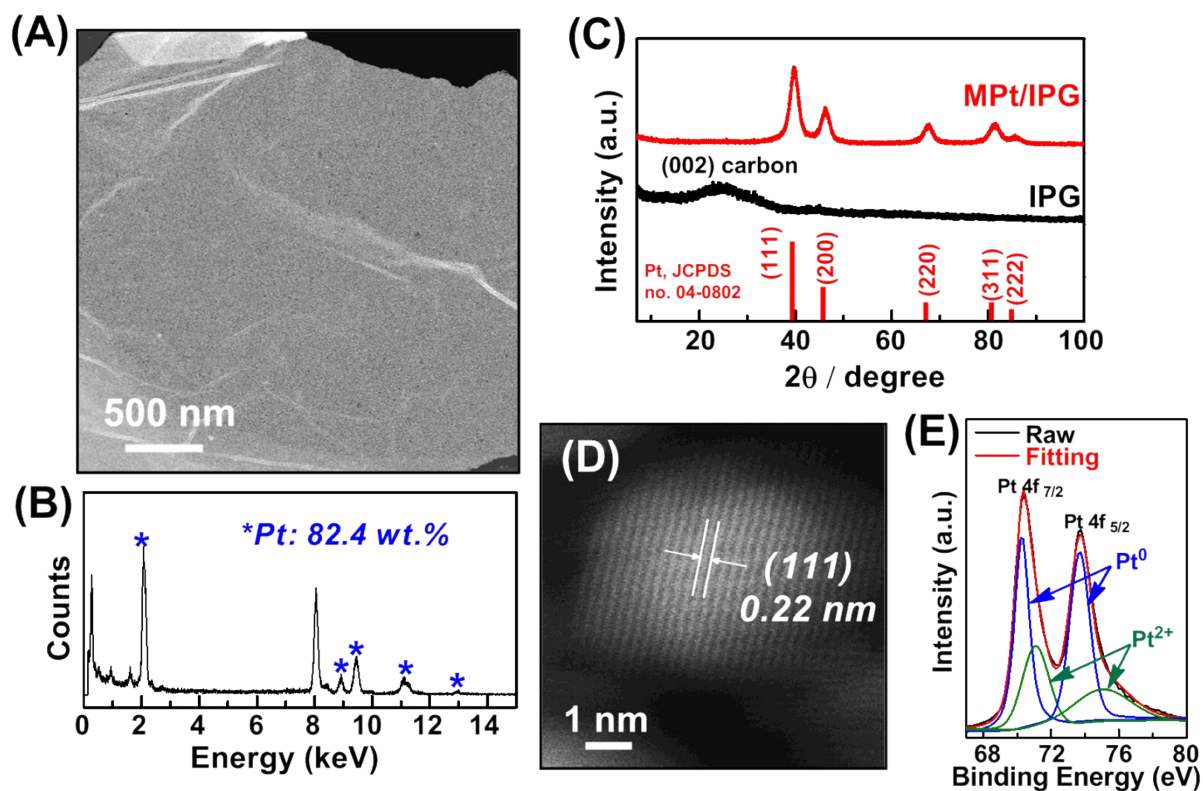


Fig. S2 (A) Representative HAADF-STEM image and (B) EDX spectrum of MPt/IPG corresponding to the STEM image in Fig. S2A. (C) Powder XRD diffraction patterns of IPG and MPt/IPG. (D) The lattice-resolved high-resolution STEM image of MPt/IPG. (E) Pt XPS spectra of MPt/IPG.

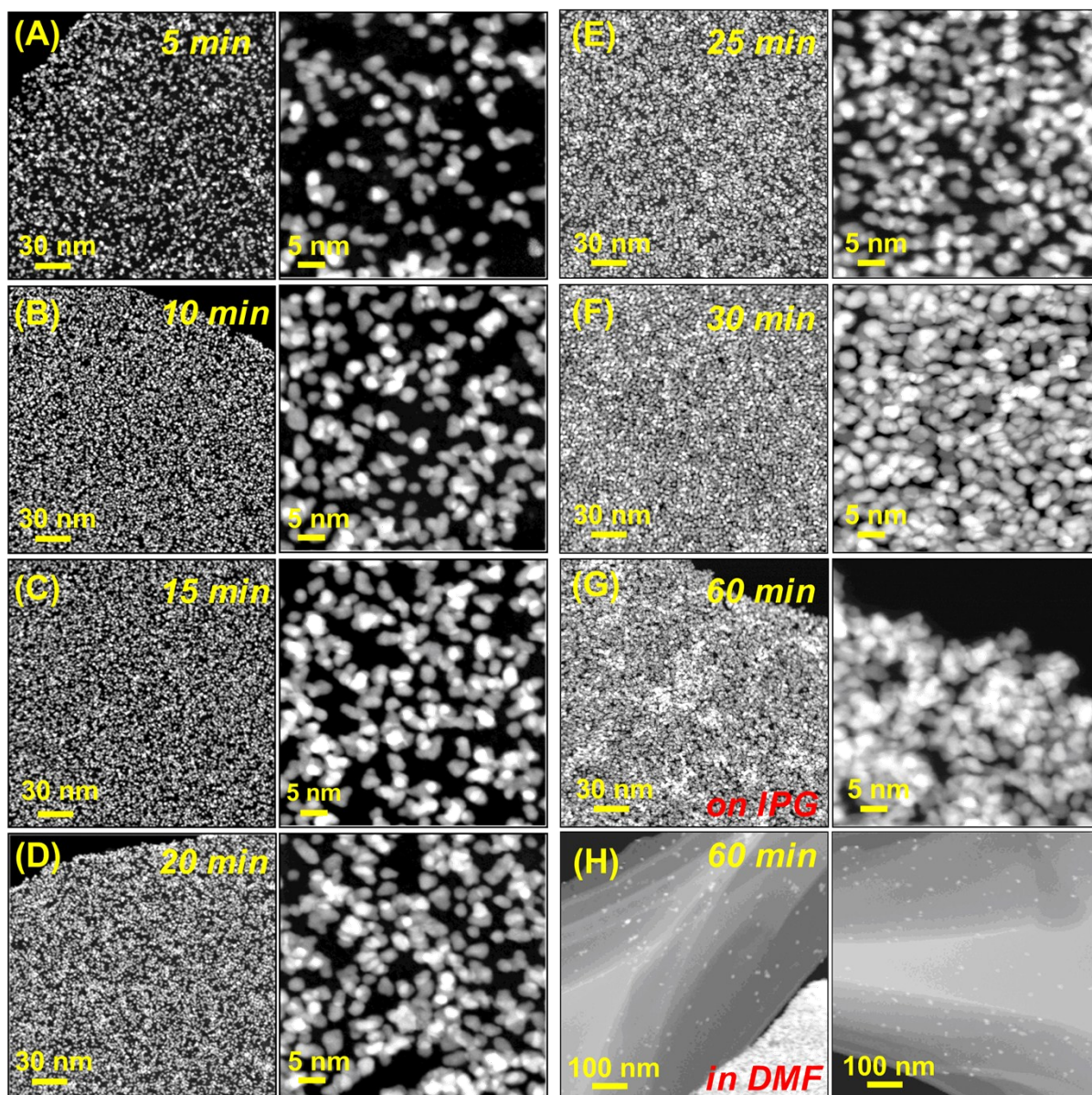


Fig. S3 Representative HAADF-STEM images of MPt/IPG according to reaction time: (A) 5 min, (B) 10 min, (C) 15 min, (D) 20 min, (E) 25 min, (F) 30 min, and (G) 60 min. (H) 60 min HAADF-STEM images of MPt/IPG obtained by the unpurified solution, exhibiting the mainly well-dispersed Pt NPs on the TEM grid.

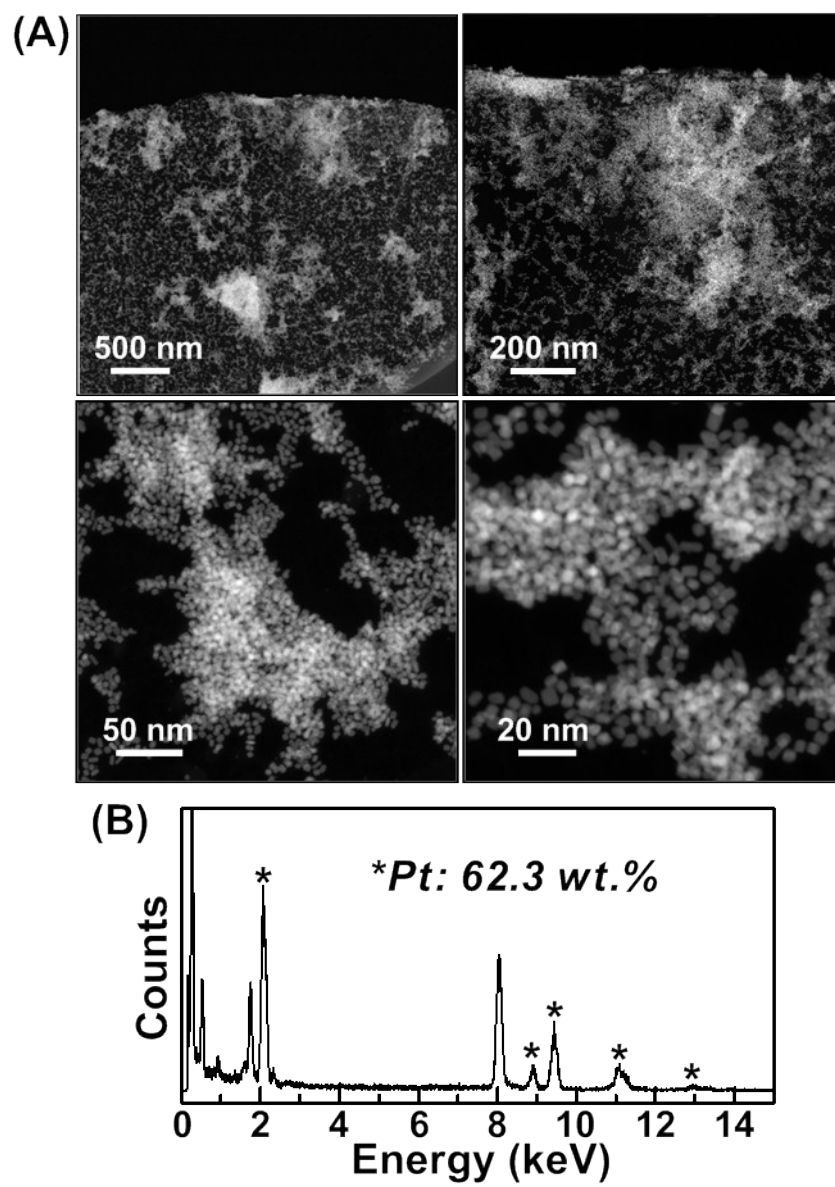


Fig. S4 (A) Representative HAADF-STEM images at different magnifications of Pt NPs/rGO. (B) EDX spectrum of Pt NPs/rGO.

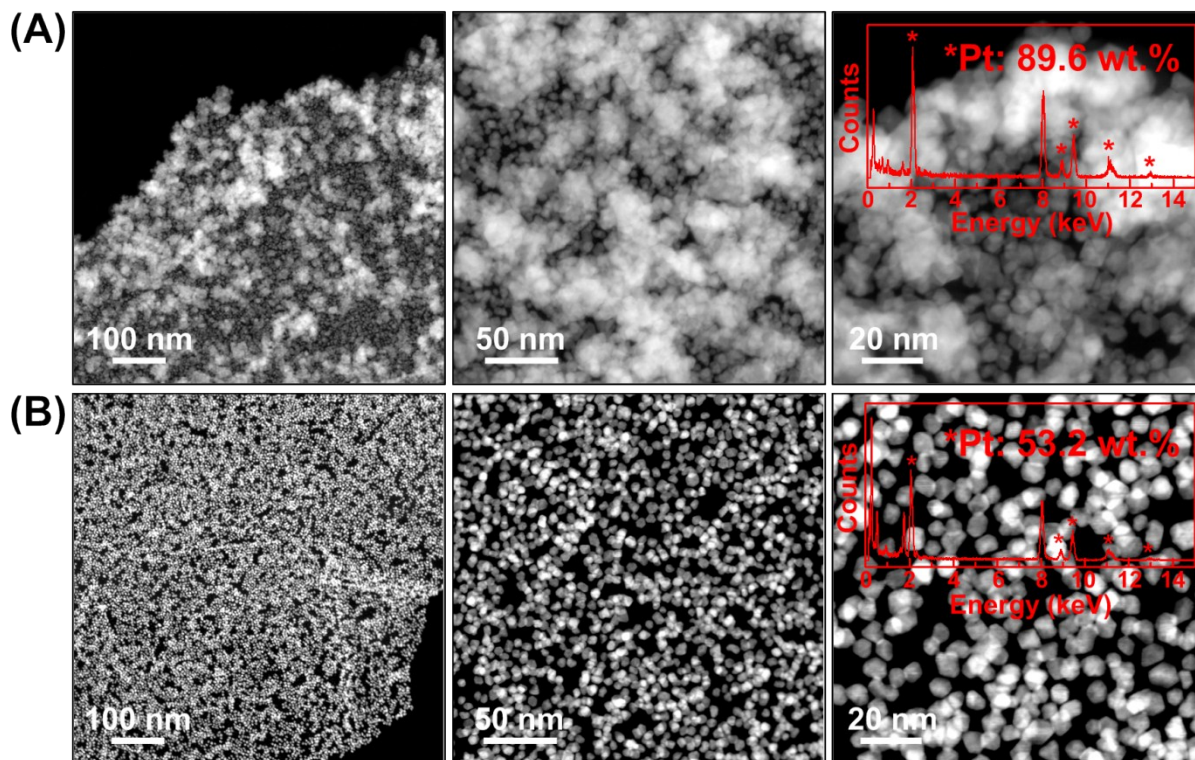


Fig. S5 Representative HAADF-STEM images of Pt/IPG at different magnifications of MPt/IPG synthesized by using (A) benzoic acid or (B) polyvinylpyrrolidone as a structure-directing agent (Inset: STEM-EDX spectra).

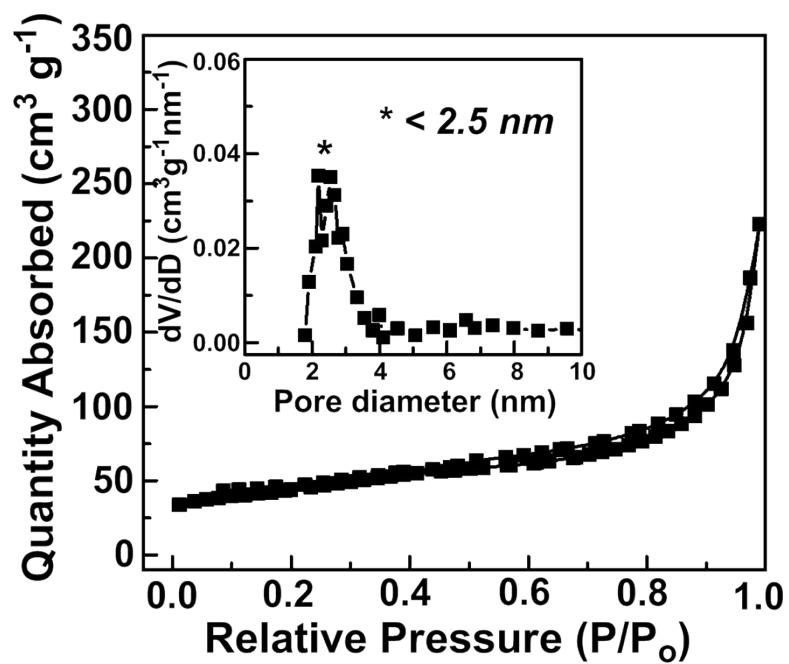


Fig. S6 N₂ adsorption-desorption isotherm of rGO (inset figure: Pore size distribution curve obtained by the BJH method of rGO).

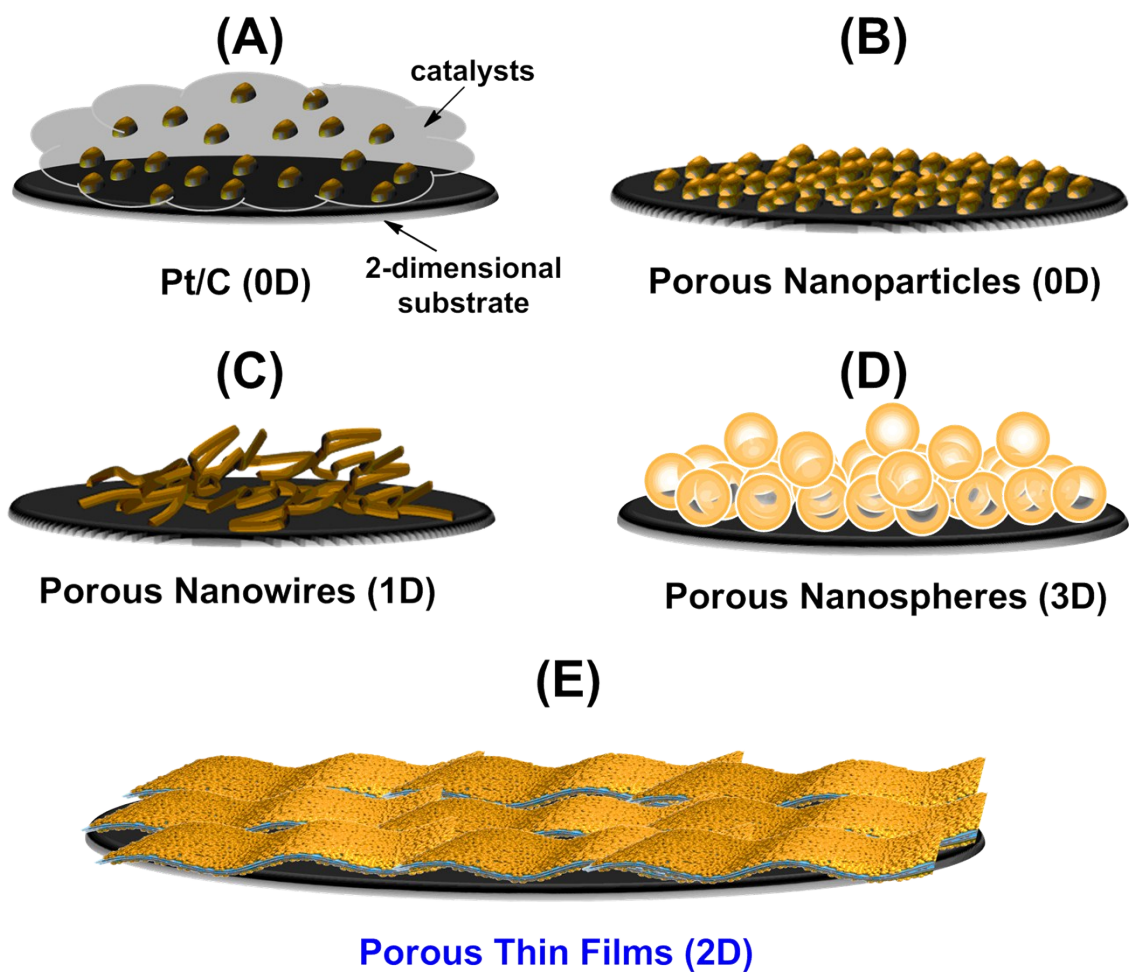


Fig. S7 Schematic illustrations of interfacial contact on the 2D surface according to the shape of catalysts. (A) Pt NPs dispersed in carbon black as a reference catalyst (0D), (B) porous nanoparticles (0D), (C) porous nanowires (1D), (D) porous nanospheres (3D), and (E) porous large-area thin films (2D).

The effective interfacial contact property of MPt/IPG originated from the 2D structure of ultra-thin film is comparable with those reported for conventional 0, 1, and 3D-structured catalysts. For example, the interfacial contact of Pt/C conventional catalyst (0D) for ORR is interfered due to the large carbon composition (~80 wt%) (Fig. 7 (A)). The porous nanoparticle (0D) and porous nanowire (1D) catalysts showed relatively lower interfacial contact properties derived from the long interval between metal catalysts because of short-range interconnection (Fig. S7 (B) and (C)). Notably, 3D structured catalysts generally have a

large size with various shapes. The size and shape factors of 3D structured catalysts can induce the large non-contact regions between catalysts, leading to lower interfacial contact efficiency (Fig.S7 (D)). In contrast, the large-area film shapes (2D) showed relatively high interfacial contact efficiency because of its intrinsic geometry property in comparison to that of 0D, 1D, and 3D nanostructures. Therefore, large-area, thin 2D structured catalyst can facilitate the high interfacial contact efficiency, which can be favorable to be the form of an efficient conducting path and to reduce an electrode thickness.

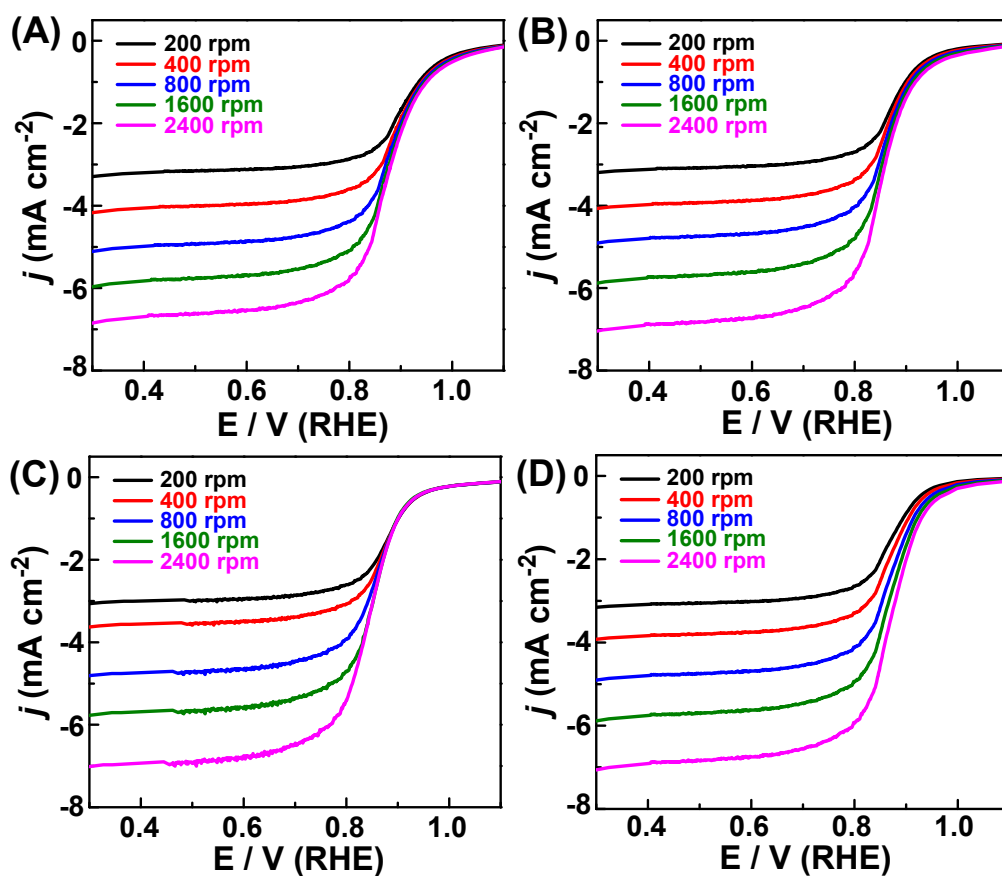


Fig. S8 ORR polarization curves of (A) MPt/IPG, (B) Pt/IPG, (C) Pt/rGO, and (D) Pt/C in an O₂-saturated 0.1M HClO₄ solution at a sweep rate of 10mVs⁻¹ and at different rotation rates (200, 400, 800, 1600, and 2400 rpm).

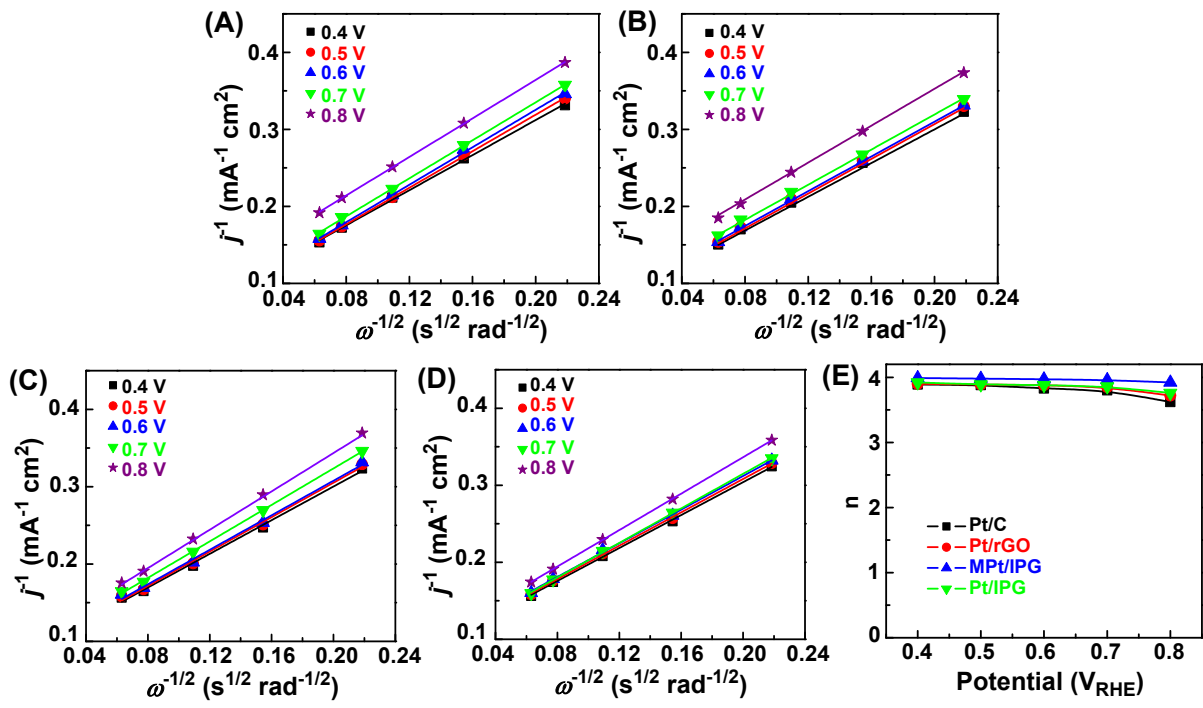


Fig. S9 Corresponding Koutecky-Levich plots of (A)Pt/C, (B) Pt/rGO, (C) Pt/IPG, and (D) MPt/IPG at different potentials (0.5 - 0.8 V). (E) Electron transfer number (n) at different potentials (0.5 - 0.8 V).

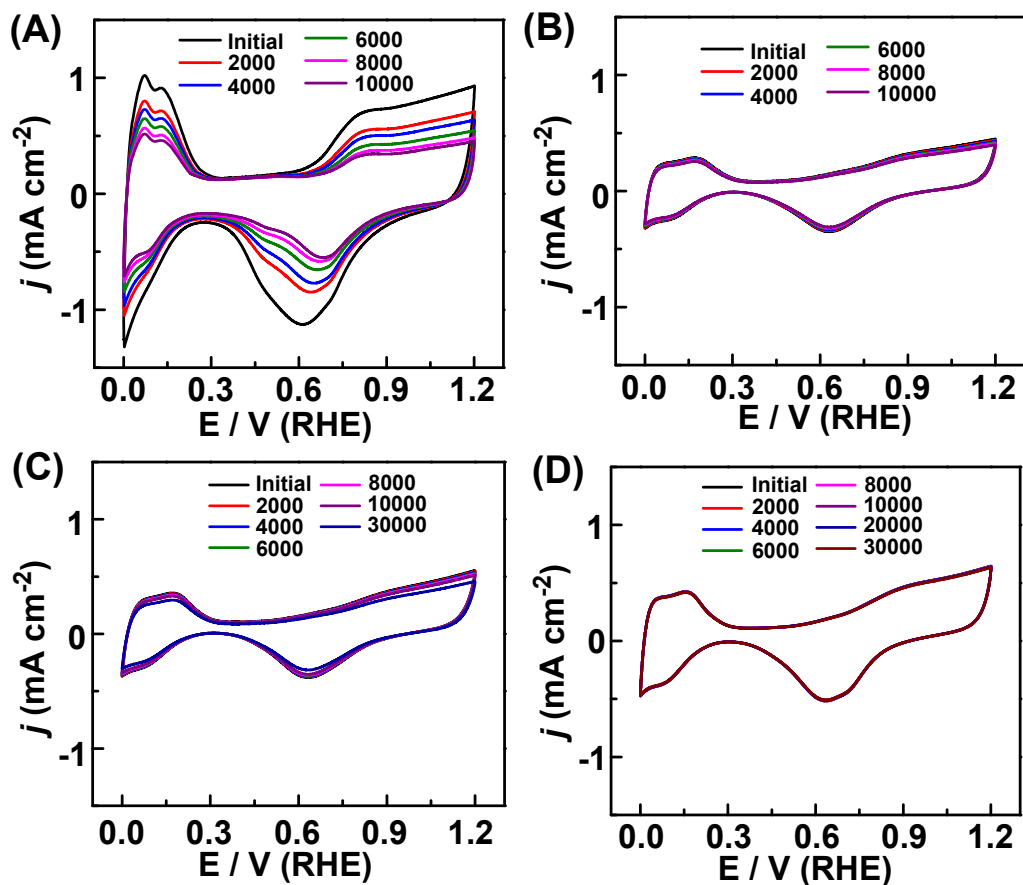


Fig. S10 Cyclic voltammograms of (A) Pt/C, (B) Pt/rGO, (C) Pt/IPG, and (D) MPt/IPG as a function of potential cycles measured at room temperature in an O₂-saturated 0.1M HClO₄ solution with a sweep rate of 50 mV s⁻¹.

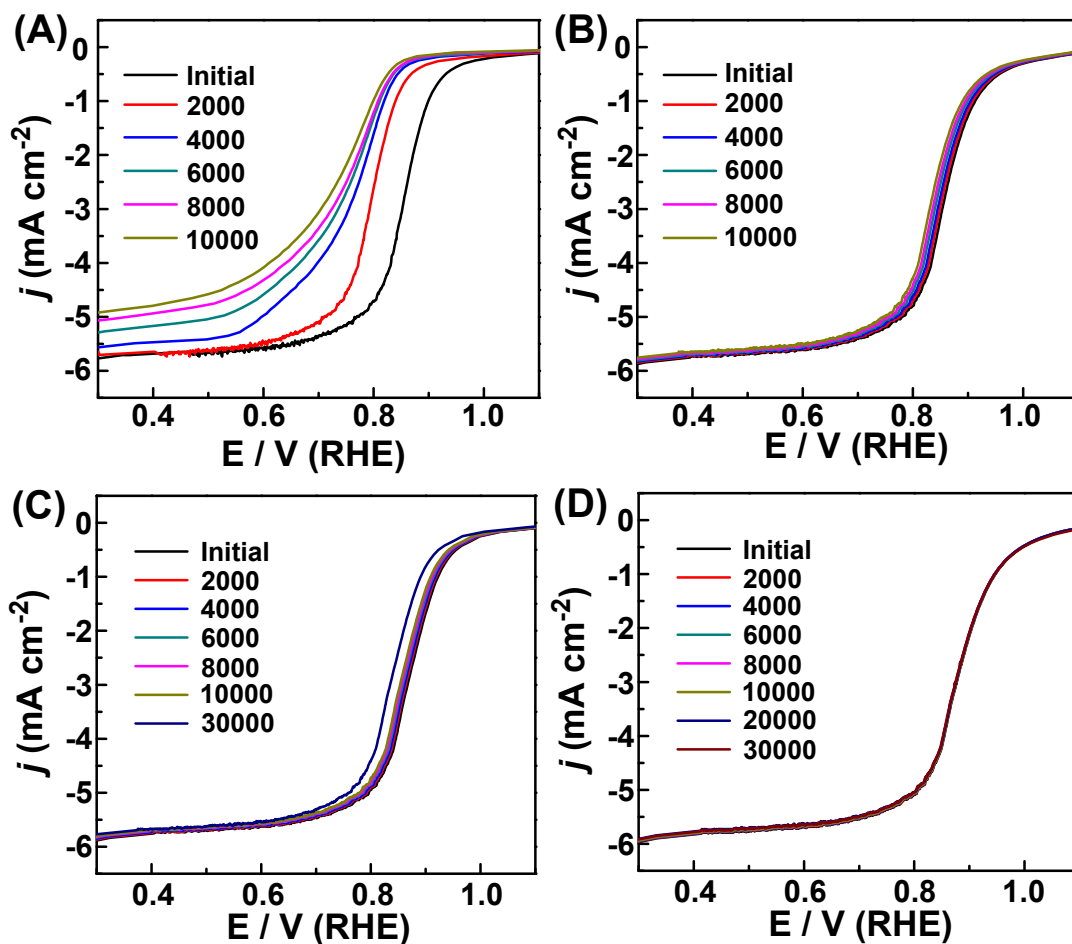


Fig. S11 ORR polarization curves of (A) Pt/C, (B) Pt/rGO, (C) Pt/IPG, and (D) MPt/IPG as a function of potential cycles measured at room temperature in an O₂-saturated 0.1M HClO₄ solution at a sweep rate of 10mVs⁻¹ and at a rotation rate of 1600 rpm.

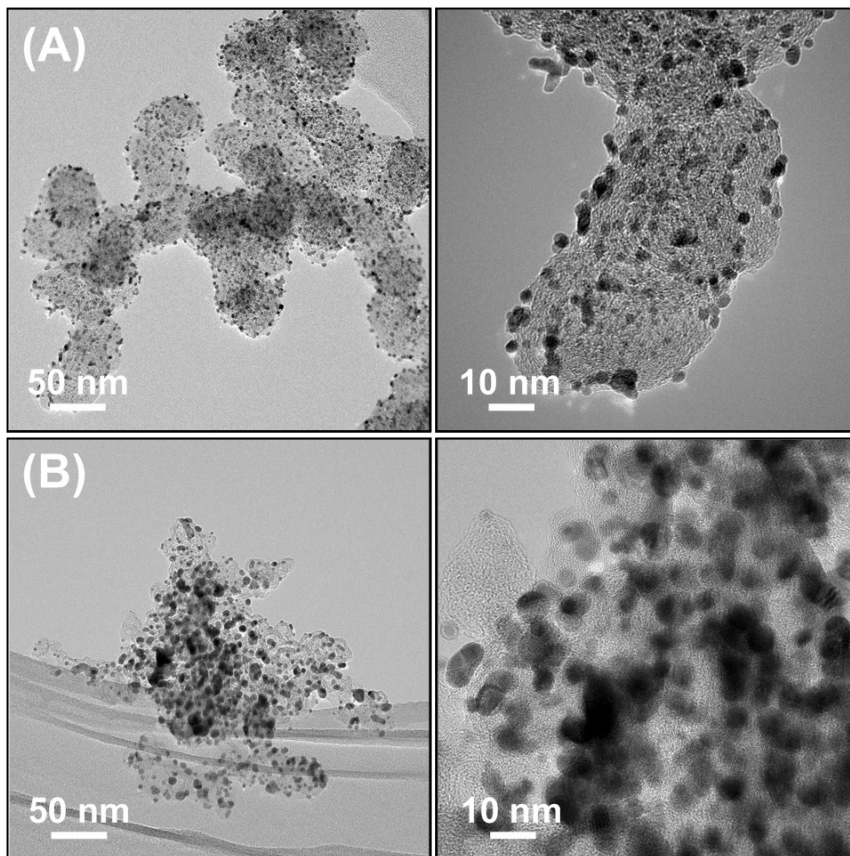


Fig. S12 TEM images of Pt/C (A) before and (B) after ADT (10k cycles) at different magnifications.

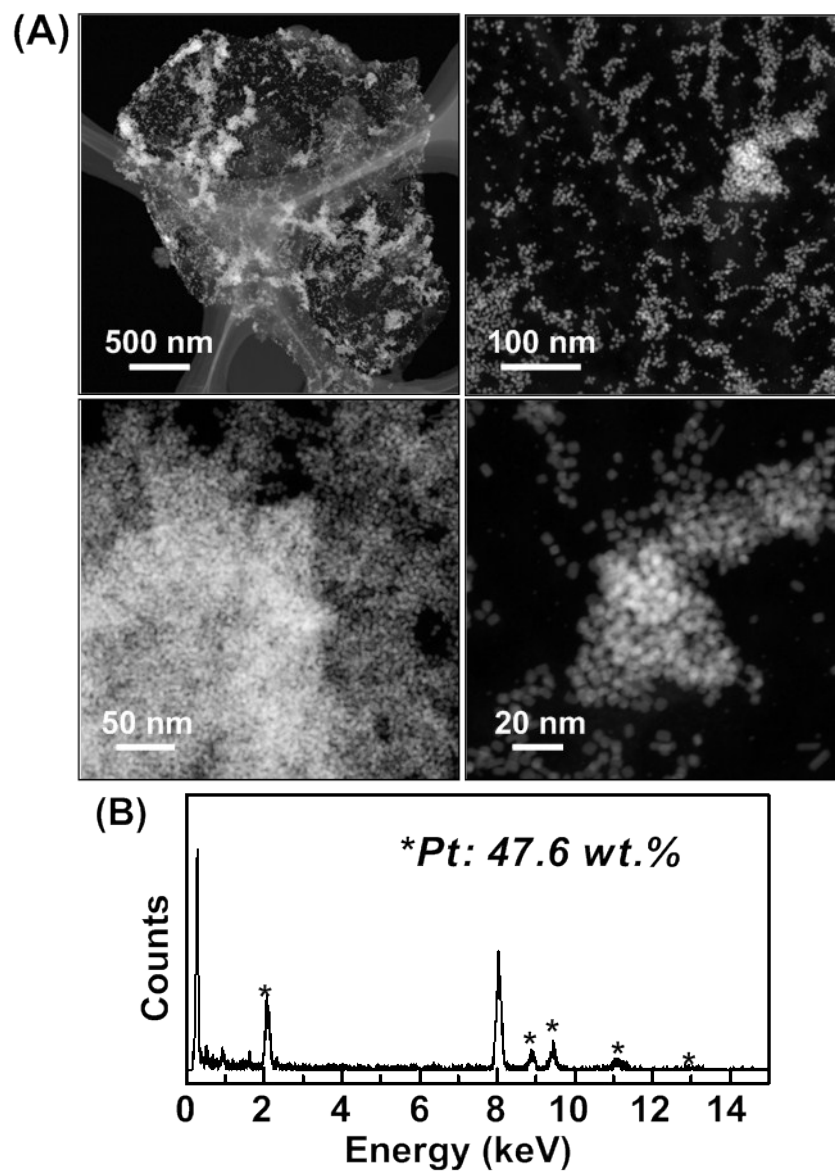


Fig. S13 (A) Representative HAADF-STEM images at different magnifications of Pt NPs/rGO after 10k cycles. (B) EDX spectrum of Pt NPs/rGO.

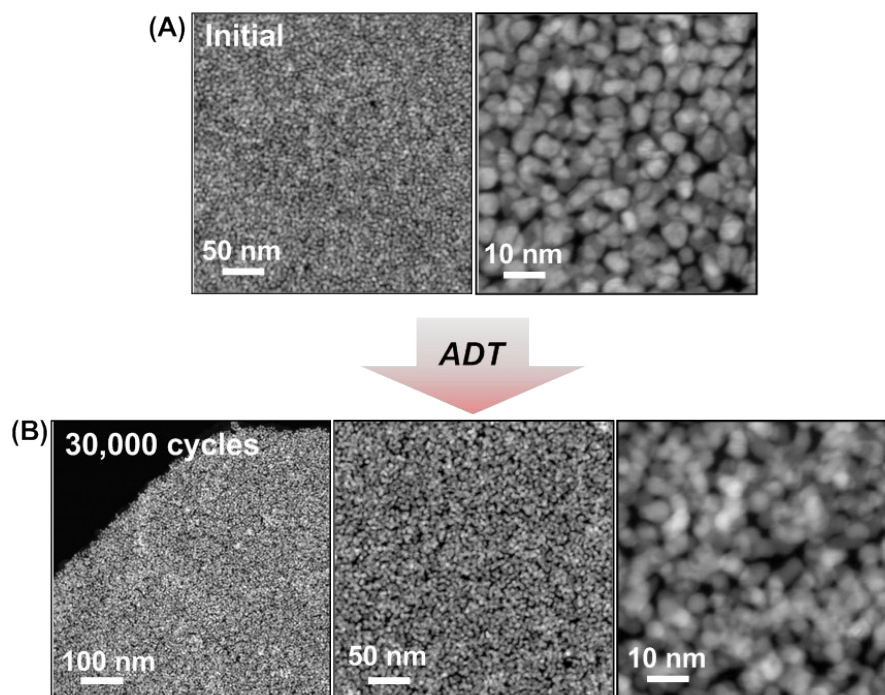


Fig. S14 Representative HAADF-STEM images of MPt/IPG at different magnifications (A) before and (B) after 30k cycles.

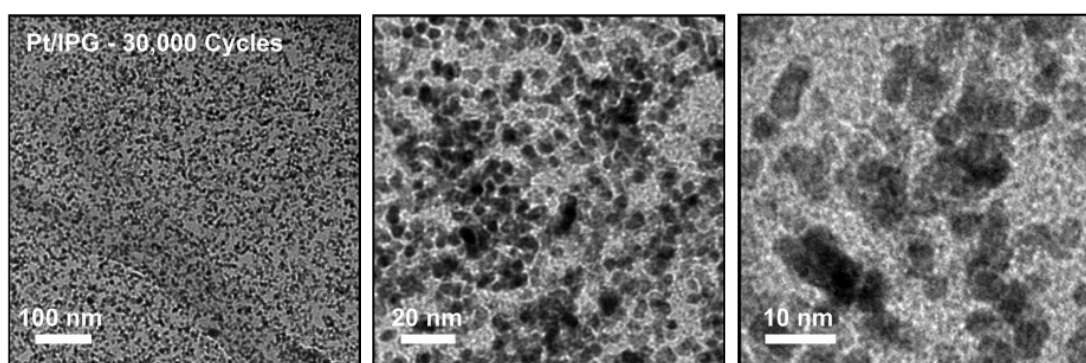


Fig. S15 Representative TEM images of Pt/IPG at different magnifications after 30k cycles of intensive durability testing.

Table S2. Comparative evaluation of electrocatalytic properties of the MPt/IPG with reported state-of-the-art Pt-based porous or nonporous structured electrocatalysts. (NA, not available)

Catalyst (Method) ^a	Support	Pt Loading ($\mu\text{g cm}^{-2}$)	ECSA ($\text{m}^2 \text{g Pt}^{-1}$)		Specific activity @ 0.9 V _{RHE} (mA cm Pt^{-2})		Mass activity @ 0.9 V _{RHE} ($\text{mA } \mu\text{g Pt}^{-1}$)		Ref.
			Initial	After ADT (Cycle #)	Initial	After ADT (Cycle #)	Initial	After ADT (Cycle #)	
			Mesoporous Pt Thin Film, MPt (In-situ)	Ionic Polymer- doped rGO, IPG	3.6	473.6	466.7 (30,000)	1.65	
Pt NPs	Ionic Polymer- doped rGO, IPG	5.8	196.2	148.7 (30,000)	1.19	0.91 (30,000)	0.40	0.30 (30,000)	This study
Pt NPs	rGO	7.5	137.1	109.6 (10,000)	0.88	1.01 (10,000)	0.21	0.15 (10,000)	This study
Commercial Pt NP	Carbon Black	14.0	72.3	29.9 (10,000)	0.23	0.07 (10,000)	0.08	0.01 (10,000)	E- TEK
Pt Nanocluster	DNA- doped GO	11.3	66.6	62.6 (10,000)	0.22	NA	0.32	NA	(4)
Pt Nanowires	S-doped Graphene	22.0	24.5	14.2 (3000)	0.68	NA	0.17	0.11 (3000)	(5)
Mesoporous Pt Nanosphere (Templating)	-	166.8	18.0	8.8 (4000)	0.40	NA	0.073	NA	(6)
Mesoporous Pt Thin Film (Templating)	-	71.4	NA	NA	0.31	NA	0.17	NA	(7)
Porous Dendritic Pt Nanotubes (Templating)	-	35.7	23.3	20.7 (4000)	0.90	NA	0.21	NA	(8)
Porous CuPt NPs (Dealloying)	Carbon Black	17.7	NA	NA	0.90	NA	0.46	NA	(9)
Porous PtFe Hollow Capsule (Templating)	-	320.0 ^b	~22	~22 (10,000)	2.3	NA	0.52	NA	(10)
Mesoporous PtNi Thin Films (Templating)	-	31.0	43	35.3 (10,000)	1.2	NA	0.51	NA	(11)
Nanoporous PtPd Alloy (Dealloying)	Carbon Black	15.7	63.5	NA	0.39	NA	0.25	NA	(12)

^a Synthetic methods for porous metal structures, ^b Membrane electrode assembly (MEA) system, the electrocatalytic measurements for almost reference catalysts were performed in 0.1 M HClO₄ solution except for ref. 8 (0.5 M H₂SO₄ solution).

References

1. K. Y. Cho, Y. S. Yeom, H. Y. Seo, P. Kumar, A. S. Lee, K. Y. Baek and H. G. Yoon, *J. Mater. Chem. A*, 2015, **3**, 20471-20476.
2. J. Y. Cheon, T. Kim, Y. M. Choi, H. Y. Jeong, M. G. Kim, Y. J. Sa, J. Kim, Z. Lee, T. –H. Yang, K. Kwon, O. Terasaki, G. –G. Park, R. R. Adzi and S. H. Joo, *Sci. Rep.*, 2013, **3**, 1-8.
3. J. N. Tiwari, K. Nath, S. Kumar, R. N. Tiwari, K. C. Kemp, N. H. Le, D. H. Youn, J. S. Lee and K. S. Kim, *Nat. Commun.*, 2013, **4**, 1-7.
4. Y. Zhou, Q. Lu, Z. B. Zhuang, G. S. Hutchings, S. Kattel, Y. S. Yan, J. G. G. Chen, J. Q. Xiao and F. Jiao, *Adv. Energy Mater.*, 2015, **5**, 1-4.
5. M. A. Hoque, F. M. Hassan, D. Higgins, J. –Y. Choi, M. Pritzker, S. Knights, S. Ye and Z. Chen, *Adv. Mater.*, 2015, **27**, 1229-1234.
6. P. –K. Chen, N. –C. Lai, C. –H. Ho, Y. –W. Hu, J. –F. Lee and C. –M. Yang, *Chem. Mater.*, 2013, **12**, 4269-4277.
7. J. Kibsgaard, Y. Gorlin, Z. Chen and T. F. Jaramillo, *J. Am. Chem. Soc.*, 2012, **134**, 7758-7765.
8. G. Zhang, S. Sun, M. Cai, Y. Zhang, R. Li and X. Sun, *Sci. Rep.*, 2013, **3**, 1-8.
9. D. Wang, Y. Yu, J. Zhu, S. Liu, D. A. Muller and H. D. Abruna, *Nano Lett.*, 2015, **15**, 1343-1348.
10. T. Tamaki, H. Kuroki, S. Ogura, T. Fuchigami, Y. Kitamoto and T. Yamahuchi, *Energy Environ. Sci.*, 2015, **8**, 3545-3549.
11. J. Kibsgaard, A. Jackson, T. F. Jaramillo, *Nano Energy*, 2016, DOI: 10.1016/j.nanoen.2016.05.005.
12. H. Duan and C. Xu, *Electrochim. Acta*, 2015, **152**, 417-424.